This is a repository copy of *Characterization of an eight element circular patch array for helical beam modes*.

Article:

Characterization of an Eight Element Circular Patch Array for Helical Beam Modes

Gary Junkin, Josep Parrón, Alan Tennant

Abstract—**This paper reports on a new method for characterizing inter-modal isolation, power penalty and reception zone area of Helical Beam antennas. As an example, an eight element circular patch array is fully characterized and its performance is critically assessed. Validation through beam measurements is accompanied with precise electromagnetic modeling using CFDTD computation on a GPU.**

Index Terms—**Helical Beams, Near-Field Measurements, Antennas, CFDTD.**

I. Introduction

HELICAL beams (HB) and the associated beam property referred to as Orbital Angular Momentum (OAM) [1] have generated considerable interest [2] in recent years and in consequence a wide diversity of proposals for so-called OAM antennas has appeared in the engineering and science literature, mostly over the last decade [3-12]. It has been mathematically demonstrated that communication range using a pair of transmit-receive OAM antennas will be limited, for example in [13] where link *transmittance* was derived as a function of distance and helical mode index. A further attempt to contribute to this mathematical debate [14] using aperture antenna theory predicts the far-field pattern and an expression for *vorticity losses*, known to be associated with beam divergence. These treatments at radio-frequencies (RF) refer to the far-field without recourse to a mechanical angular momentum calculation, a property of the beam that would appear to be incidental at RF. Viewed from an Euler equation perspective, the HB is a quadrature combination in time of two spatially orthogonal transverse modes that propagate axially as a beam and excite the corresponding two modes in the HB receive antenna. For modal communication over air to be successful requires a sophisticated antenna that is capable of discriminating between multiple helical modes, for example using the fact that a $m-$cycle azimuth variation excites a radial Bessel variation J_m in a coaxial resonator in [6].

Helical beams can enable both frequency and polarization

G. Junkin and J. Parrón are with the Department of Telecommunications & Systems Engineering, Universitat Autònoma de Barcelona, Catalunya, Spain. Gary.Junkin@uab.cat

A. Tennant is with the Department of Electronic and Electrical Engineering at The University of Sheffield, U.K.

diversity over distances that are best quantified in terms of the Rayleigh range, $z_R = \pi w_0^2 / \lambda$ where w_0 is a radius called beam waist. By comparison, the far-field distance is a boundary distance that is only 2.55 times the Rayleigh range, but the concept of far-field is usually understood as a distance much greater than this minimum value. As concluded in this paper, HB mode transmission using concentric modes could be extended to ten times the Rayleigh range for the first HB mode, at the sacrifice of efficiency.

In terms of antennas, a popular OAM antenna typology is the uniform circular array (UCA), first suggested in [3]. One of the earliest examples having a small circular aperture array was the 8-element linearly polarized patch array [4] that emits a single $m = \pm 1$ OAM mode. Ring-resonators can also be used to create the angular mode, for example the circularly polarized OAM antenna in [5] can simultaneously emit both m = ±3 modes, but this relies on a reflector antenna to provide directivity. A multimode circularly polarized helical beam antenna design based on coaxial resonators was recently proposed in [6]. Collimated beam solutions based on radial line slots arrays (RLSA) [7] have been proposed for Bessel beam generation [8] and related OAM modes. Another beam technology borrowed from optics, the circularly corrugated flat plate structure, has recently been shown to support OAM modes [9] with the so called bull's eye antenna. Many other approaches are currently being reported, such as Rotman lenses [10], horn antennas [11] and flat-plate antennas [12].

This paper however deals with HB system characterization, which is presented from the perspective of Fourier Optics [16] using a method with roots in antenna measurement theory [17]. Whereas previous characterizations of HB antennas have typically performed standard antenna measurement techniques on the test antenna using a standard probe antenna [12], the approach here is fundamentally different and tests the complete HB system consisting of the transmit and receive pair of HB antennas. Furthermore, in order to gauge error levels, rigorous testing is performed with accurate S-parameter beam measurements referenced to detailed numerical simulation of the HB antenna. Beam purity is quantified in terms of inter-modal and intra-modal isolation as a function of frequency, communication range and reception zone area.

The antenna system under test (ASUT) consists of a set of three separate antennas, each of which is an eight element UCA of micro-strip patches [4]. These UCA antennas were supplied as fabricated units and serve here as a technological reference for what is presently available in the microwave

bands. Since the UCA antennas in the ASUT are only capable of emitting a single helical mode then two with mode $m = -1$ (M1) and one with mode $m = +1$ (P1) are configured to perform the equivalent transmission measurements M1-M1 and M1-P1.

Full electromagnetic simulation in three-dimensions (modeling) is carried out to compare expected behavior with measurement in order to confirm that errors have been correctly controlled. In particular the CFDTD [18] method running on a GPU provides fast and accurate modeling of the input impedance and radiated helical beams, and permits a precise determination of dielectric constant and loss tangent of the substrate found in the antennas (FR-4), based on wideband comparison with measured S-parameters. The excitation on the patch edges is subsequently calculated accurately in order to explain performance.

Beam measurements with a two-dimensional scanner are carried out to confirm calculated behavior and to determine mode purity coefficients or the so-called *topological charge* as a function of frequency. Correspondence between these modal purity coefficients and the inter-modal isolation obtained from laboratory S-parameter measurements is presented and in turn is compared with a new method based on convolution for completely characterizing inter-modal isolation, power penalty and reception zone area.

II. HELICAL BEAM CHARACTERISTICS

In the following we briefly outline three methods in which HB characteristics may be quantified in some sense. The first is commonly used in optics and involves the concept of topological charge (TC) [15]. It is useful for determining the helical mode content of a beam and the frequency dependence of each mode. The second method is a graphical representation based on beam profile plotted in polar coordinates and is commonly found in publications on OAM antennas. In addition to this graphical representation, the field amplitude variation $f(\phi)$ with azimuth angle ϕ can be quantified in a way similar to VSWR as $|f_{max}|/|f_{min}|$ and the peak phase deviation can be calculated with respect to the modal variation $e^{jm\phi}$. Neither of the aforementioned methods directly quantifies the modal coupling and isolation in terms of received signal; they are essentially indirect indicators of beam performance. Additionally, modal coupling and isolation are not represented as a function of position in the transverse plane, although this could be calculated by changing the topological axis definition. Inspired by the measurement results presented in section V, a third method based on the convolution of the helical beam mode is proposed here to show how the position of greatest modal isolation drifts in the transverse plane as a function of frequency. Essentially, the optimum reception location is dependent on frequency when the antenna is behaving poorly in terms of beam purity.

As inter-modal isolation requires two modes of the same order, and as the antenna under test supports only a single mode, a substitution method is used with two antennas of opposite mode number. Furthermore, since the beam quality

of the UCA antennas in this case are not ideal, the characterization of the 2-D ASUT beam patterns demonstrate how inter-modal isolation and reception zone area change with frequency.

A. Mode Purity of topological charge

The mode purity coefficient $c_m(\omega)$ at harmonic frequency ω for mode number m is defined [15] for a single directional component $E_t(\omega)$ of the vector electric field in the transverse plane cutting through the helical beam as

$$c_l(\omega) = \frac{2\pi \int_0^\infty \left|\frac{1}{2\pi} \int_0^{2\pi} E_t(\rho,\phi) e^{jm\phi} d\phi\right|^2 \rho \, d\rho}{\oiint |E_t|^2 \, dA} \tag{1}$$

Inherent in this definition is an alignment of the topological z-axis through some point (x_0, y_0) that defines ρ in terms of the transverse coordinates (x, y).

B. Beam Polar Profile

The amplitude and phase of the helical beam profile is plotted in polar coordinates. The measurement is taken with a standard probe at a range that is sufficiently large to avoid antenna interactions, but sufficiently small to avoid truncation effects and is usually several antenna diameters distant. The amplitude and phase are plotted as a function of azimuth angle, where a polar radius is chosen that usually corresponds to maximum beam amplitude. The electrical beam center must previously have been calculated based on linear profiles in the horizontal and vertical axes.

C. Mode Convolution Functions

Planar near-field antenna measurement techniques [19] already establish the mathematical foundations for the signal received by a standard probe, in terms of an element by element product in K-space between plane-wave spectra of the probe and the antenna, which is a convolution in measurement space. In this particular application the signal field is received with a HB probe antenna having the corresponding helical mode, and the cross coupling measurement between modes requires the transmission of a particular helical mode and the reception of a distinct helical mode probe. The convolution in space is a field overlap integration that can be efficiently and accurately evaluated numerically by the fast Fourier transform (FFT). Measurement of modal isolation over the entire reception zone area is therefore easily calculated and its verification over the frequency band is a further measure of beam quality.

In this new beam assessment method the mode beam pattern $\overrightarrow{f_{M1}}$ for antenna M1 is measured in the transverse plane with an ideal probe at a distance $z/2$ and this is convolved separately with the $\overleftarrow{f_{M1}}$ and $\overleftarrow{f_{P1}}$ probe patterns orientated in the negative z direction, as indicated by the arrows. By examination of Fig.1 (a) and (b), the P1 probe pattern viewed in the negative z direction $\overleftarrow{f_{P1}}$ is identical to the M1 pattern viewed in the positive z direction $\overrightarrow{f_{M1}}$, then to calculate the received field pattern f_{M1P1} at z by probe antenna P1 we have, as shown in Fig.1 (d) and (f)

$$f_{M1P1}(x,y,z) = \overrightarrow{f_{M1}}(x,y,z/2) \otimes \overleftarrow{f_{M1}}(x,y,z/2) \quad (2)$$

The M1 probe pattern viewed in the negative z direction $\overleftarrow{f_{M1}}$ is a rotated version of $\overrightarrow{f_{M1}}$ about the y-axis

$$\overleftarrow{f_{M1}}(x,y,z) = \overrightarrow{f_{M1}}(x,-y,z) \quad (3)$$

The received field pattern with probe M1, as shown in Fig.1 (c) and (e) is hence

$$f_{M1M1}(x,y,z) = \overrightarrow{f_{M1}}(x,y,z/2) \otimes \overrightarrow{f_{M1}}(x,-y,z/2) \quad (4)$$

As phase is accumulative in the convolution process then the f_{M1} pattern is measured at $z/2$ in order to calculate f_{M1M1} and f_{M1P1} patterns at distance z. The convolution is performed with the FFT as follows where $\mathfrak{F}$ is the Fourier transform

$$f \otimes g = \mathfrak{F}^{-1}\big(\mathfrak{F}(f)\mathfrak{F}(g)\big) \quad (5)$$

In practice antennas M1 and P1 may have slight differences due to fabrication and additionally when a waveguide probe is used the patterns should strictly be probe compensated using the measured waveguide probe pattern. However, since we are primarily interested in the paraxial performance for on-axis reception then we can omit this detail to good approximation.

An ideal mode convolution function (MCF) corresponding to the measurement of $f_{M1M1}(x,y,z)$ can be calculated for a theoretical beam as follows. The beam scalar aperture field A_m for mode m is described as

(a) $\mathrm{Re}\left(\overrightarrow{f_{M1}}(x,y,z/2)\right)$ (b) $\mathrm{Re}\left(\overrightarrow{f_{P1}}(x,y,z/2)\right)$

(c) $\mathrm{Re}\left(f_{M1M1}(x,y,z)\right)$ (d) $\mathrm{Re}\left(f_{M1P1}(x,y,z)\right)$
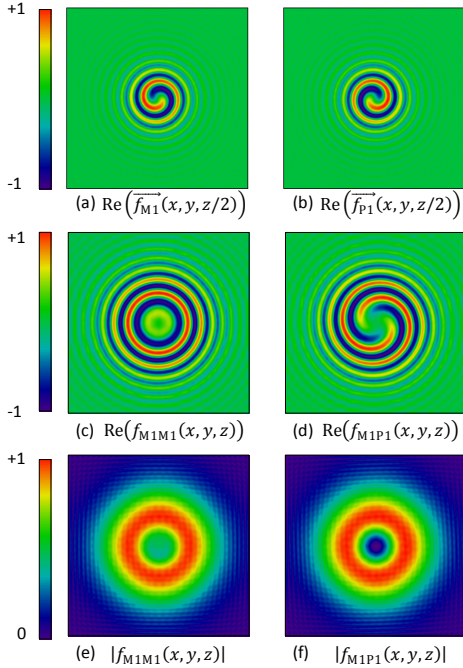
(e) $|f_{M1M1}(x,y,z)|$ (f) $|f_{M1P1}(x,y,z)|$

Fig. 1. Ideal beam patterns shown on a linear scale: (a) M1 and (b) P1 viewed in +z direction at half the distance z. (c) Real part of the MCF for M1-M1. (d) Real part of MCF for M1-P1. (e) Amplitude of MCF M1-M1. (f) Amplitude of MCF M1-P1 showing zero sign in central zone.

$$A_m(\rho,z=0) = \exp(-a\rho^2)\exp(jm\phi) \quad (6)$$

This beam can be propagated a distance $z/2$ in an approximate fashion using the propagation filter [16] $H(k)$ in conjunction with the Fourier Transform, where

$$H(k_x,k_y) = \exp\left(-j\frac{z}{2}\sqrt{k_0^2 - k_x^2 - k_y^2}\right) \quad (7)$$

The field $f_m(z/2)$ at distance $z/2$ is given by

$$f(x,y,z/2) = \mathfrak{F}^{-1}\big(\mathfrak{F}(A_m)H(k_x,k_y)\big) \quad (8)$$

where the size of the FFT determines the precision of the integration carried out in equation (8). An ideal MCF is then calculated with equation (2) or (4) and can be used for comparison in section V on beam measurements, where it is shown to agree well with antenna measurements at distances of 150 mm and 300 mm. Intermodal isolation is defined as $I_{MP1} = 20\log_{10} f_{M1P1}/f_{M1M1}$. Reception zone is defined here as the area over which intermodal isolation I_{MP1} is better than 10 dB. Power penalty is defined here as the ratio of maximum power received over the beam extent to the power received in the reception zone. It is experimentally demonstrated in section V.D that MCF gives a good approximation of intermodal isolation, modal power penalty and reception zone area.

III. THE HELICAL BEAM ANTENNA DESIGN

A review of the design of the UCA antennas is presented in the following in order to appreciate some design difficulties that will explain the non-ideal characteristics appearing later in measurements.

A schematic of the M1 ($m = -1$) UCA antenna, which was reported in [4], is shown in Fig. 2a with corresponding parameters in Table I. The design approach was inspired by feeding the array of patches with a cyclic phase excitation $e^{jm\phi}$. However, in this design there is no possibility of independently exciting the opposite mode P1 ($m = +1$).
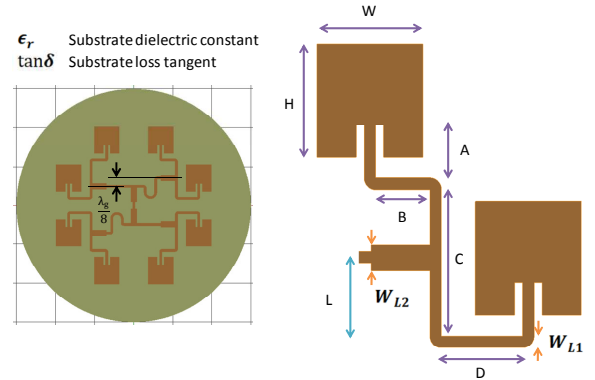

Fig. 2a. The eight element UCA of patch antennas (left) and first quadrant of connected patches (right).

The feed network can be understood by dividing the array into 4 quadrants, where quadrant patch-pairs are fed with four identical power dividers orientated in the horizontal direction. The vertical location of the power divider provides a +45° phase difference at the respective patch inputs, when viewed in the anticlockwise sense for the antenna as shown. Since two corners are present in both paths, the required offset difference can be calculated to very good approximation for modes $m = \pm 1$ as

$$L_m = \frac{C}{2} - \frac{D-B}{2} - m\frac{\lambda_g}{16} \qquad (3)$$

where λ_g is the microstrip wavelength at design frequency.

The first and third quadrants have a further +90 phase by virtue of the looped line segment on one branch of the transformer outputs. Quadrants three and four have an additional 180º as their corresponding patches are fed from the top edge. The patch phases are hence sequenced by +45º. The opposite helical mode $m = +1$ with offset L_{+1} has the looped lines swapped to the opposite quadrants; effectively a rotation of the structure by 180º with respect to the vertical axis. The vertical distance between horizontally orientated transformers as indicated in Fig. 2a should be exactly $\frac{\lambda_g}{8} = 2.134$ mm at design frequency but was 2.24 mm in the design provided, corresponding to an difference of about 100 μm. The array radius is approximately 18 mm for each patch, where some adjustments appear to have been made in the design process [4]. The line L_1 characteristic impedance is approximately 100 Ω and the corresponding transformer L_2 impedance is 70.7 Ω. The patch parameters (height, width and slot length) appear to have been designed for 200 Ω patch input impedance by mistake, resulting in a 25 Ω impedance at the input port.
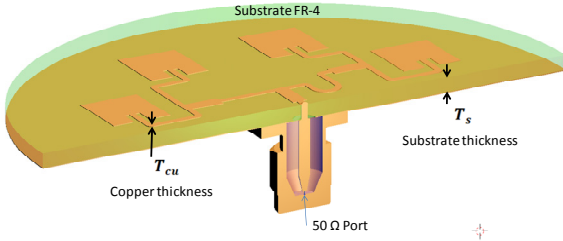

Fig. 2b. The 3D model used in CFDTD calculations.

Table I
ANTENNA PARAMETERS AND DIMENSIONS (mm)

ϵ_r	$\tan\delta$	T_s	T_{cu}	W_{L1}	W_{L2}	$\frac{\lambda_g}{16}$
4.25	0.0175	1.55	0.035	0.707	1.652	1.074
A	B	C	D	W	H	L
3.3	3.34	9.04	5	6.5	7	4.764

ANTENNA MODELING WITH CFDTD AND FEKO

Helical beam antennas (HBA) are inherently electrically large structures and their modeling times are often inconveniently long on desktop computers. Here these times are further exacerbated when transmit and receive antennas are modeled as a transmit/receive pair. The advantage of CFDTD is that it is highly efficient when combined with a GPU [20] and is particularly suitable for modeling printed circuit board (PCB) antennas that are orientated along a grid plane, where dual PCB antennas are parallel and not separated by more than several antenna diameters. The principal advantage of FEKO [21] is that it permits arbitrary orientation of the geometry. Accurate modeling with CFDTD on a Titan-XP GPU have been reduced to under 3 minutes. CFDTD also covers an octave frequency range that is advantageous for electrical parameter estimation. For example, the economic

FR-4 substrate is not well suited for 10 GHz operation because of its relatively high losses, and hence sufficiently accurate parameter values for dielectric constant and loss-tangent are not available at this design frequency. The antenna input impedance is sensitive to both these parameters as well as the mesh size used in the numerical modeling. Thus two distinct numerical simulators were employed in order to have confidence in both the level of numerical modeling errors and in the estimated electrical parameters.
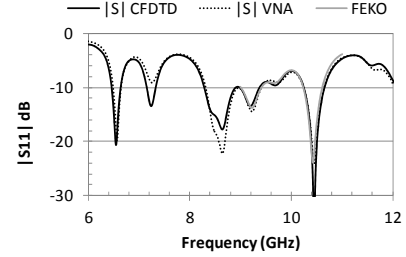

Fig. 3. The M1 UCA antenna $|S_{11}|$ parameters, showing comparison between VNA measurement, CFDTD and FEKO calculations.
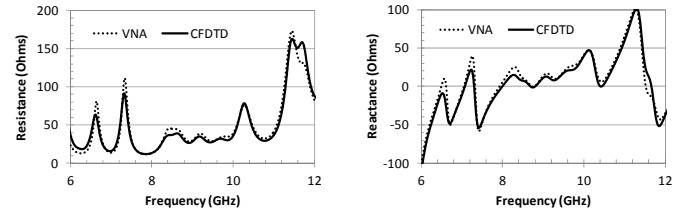

Fig. 4. The M1 UCA antenna input impedance, showing comparison between VNA measurement and CFDTD calculation.
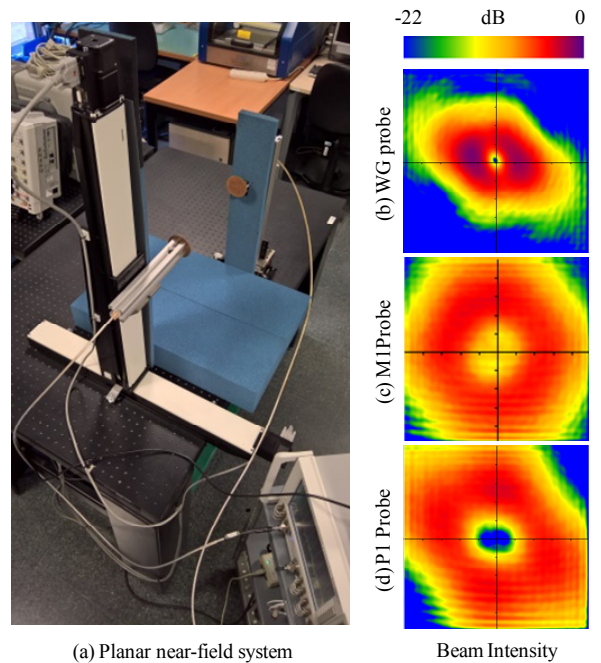

Fig. 5. Comparison of beams received at 9.6 GHz from a M1 antenna using the scanning system in (a) with probes: (b) Open ended waveguide, (c) Identical M1 antenna, (d) Mirror image P1 antenna. Intensity is shown on a 22.5 dB range. Scan window is 500 mm. Scan distance is 300 mm.

A. Modeling Input port S-parameters

Fig.3 shows the level of accuracy attained in the modeling

of the antenna input port S-parameter S_{11} using CFDTD and FEKO. In order to get such good agreement with measurement, it was found necessary to model the PCB tracks with the feed pin and coaxial connector as an integral part of the antenna model as shown in Fig. 2b. The feed pin of the SMA connector has a 1.3 mm internal diameter and the external length passing through the substrate is 0.7 mm diameter for connection to the 0.7 mm 100Ω lines L_1 of width W_{L1}.
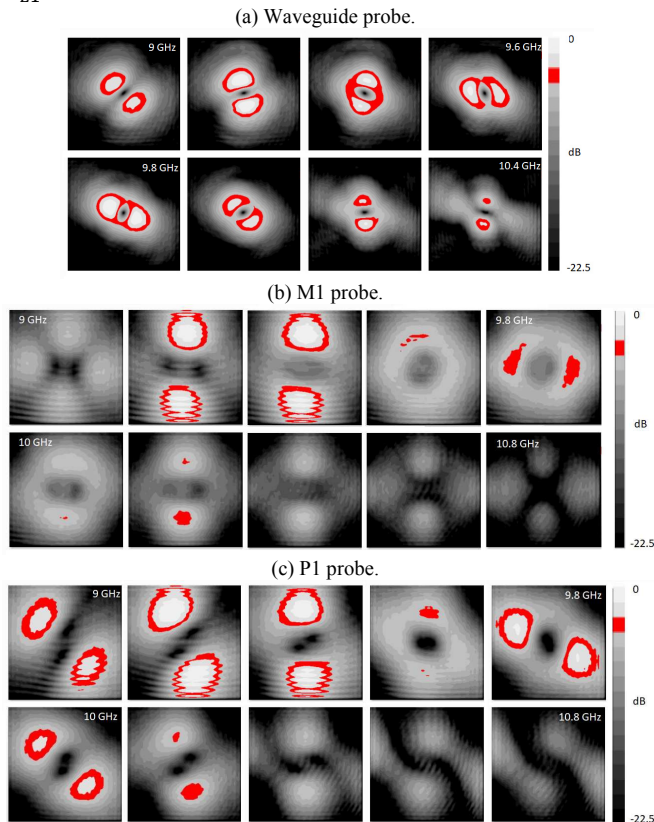
(a) Waveguide probe.

(b) M1 probe.

(c) P1 probe.

Fig. 6. Reception of helical mode M1 with three probe types as indicated, for a scan distance of 300 mm, over 9 to 10.8 GHz. Scan window is 500 mm and grey-scale range is 22.5 dB (1.5 dB per grey level). Red indicates -3 dB.

Fig. 4 shows the corresponding input impedance of the antenna referenced to the input plane of the SMA connector, confirming that the real part of the impedance is close to 25 Ω between 9 GHz and 10 GHz, which indicates a patch antenna input impedance of about 200 Ω. Subsequently performed beam measurements confirm that the best helical beam frequency is 9.6 GHz.

IV. BEAM MEASUREMENTS

The system shown in Fig. 5 consists of a Galil controlled precision Newmark double axis planar scanner and an Agilent PNA-X network analyzer measuring S_{21} from 9 GHz to 11 GHz in 100 MHz steps over a 500×500 mm scan window, with a scan time of approximately 50 minutes. Measurements were performed at 150 mm and 300 mm from the antenna (corresponding to 2.29 and 4.58 times the Rayleigh range for an equivalent beam waist radius of 25 mm). As shown in Fig. 5, three types of probe antenna were used in sequential sets of

measurements; a rectangular open-ended waveguide probe, a M1 antenna probe and a P1 antenna probe. The colored inset beam profiles at 300 mm shown in Fig. 5 correspond to the frequency 9.6 GHz of best performance in terms of beam uniformity. As indicated qualitatively by the color-tables in Fig. 5 and later in detail in both Fig. 12 and Fig. 13, at 300 mm distance the M1 received signal drops by approximately 7 dB at the center but the P1 received signal is about 15 dB below this over an area corresponding to the size of the antenna. This means that the intermodal isolation between modes $m = \pm 1$ is approximately 15 dB between 9.6 and 9.8 GHz, although there is a penalty of about 7 dB with respect to maximum received signal which is practically identical for probes M1 and P1. A linear dipole would therefore not be able to distinguish between either the M1 or P1 modes even though it would receive a strong signal at a radius of 60 mm as indicated in Fig. 7. Included in Fig. 7 are the cross-polar levels for the M1 antenna, which are more than 15 dB down with respect to co-polar levels.

The frequency variation of the mode patterns is shown in Fig. 6 for illustration purposes over a frequency range (9 GHz to 10.8 GHz) much larger than the expected impedance bandwidth of the patch array. It illustrates the fact that the central null in M1-P1 begins to split into two components from about 200 MHz either side of 9.7 GHz. This means that the position for optimum inter-modal isolation, and best reception zone area, is frequency dependent with a positional drift in the order of several antenna diameters. Some reflection effects from the table are apparent in the beam measurements, particularly below 9.5 GHz in the case of probes M1 and P1, where their off-axis radiation patterns are substantially worse at these frequencies. The expected circularly symmetric doughnut shape of the M1 beam is substantially distorted by the relatively poor VSWR of the patch array excitation.

A. Patch excitation determined by CFDTD

The CFDTD predicted patch excitation viewed at a small distance from the patch slots that are opposite their respective feeding lines is useful for antenna tuning. Fig. 8 shows the variation in patch excitation field for the 10 GHz design frequency is a high VSWR of 2.86 with a corresponding phase error range of -18/+24 degrees. At 9.6 GHz the situation is 25% better with a VSWR of 2.2 but the phase error range of -30/+18 degrees is worse. Because of the small array radius of 18 mm, the feed network is excessively close to the patches and in particular line C strongly couples to its adjacent patch. The line corners also contribute strongly to the high VSVR on the feed lines, which as a result causes the non uniform and frequency sensitive patch excitation seen in Fig. 8. This explains the degraded elliptical shape of the helical beam that was seen in Figure 5(a). The optimum frequency is 4% below design frequency, because of the inaccurate value of dielectric constant used in the design.

B. Beam polar profile

The measured beam amplitude and phase polar variation over a circle of radius 60 mm is shown in Fig. 9 and

demonstrates that at a distance of 150 mm the beam amplitude has a VSWR of 1.75 at 10 GHz and corresponding phase error range of $-25/+36$ degrees. This agrees well with the CFDTD predicted patch excitation at 10 GHz. Interestingly in Fig. 9 (b) at 9.6 GHz the measured VSWR is reduced by 30% to 1.22 while the phase errors are now smaller with a range of -22/+28 degrees. Given the limitations on space for the UCA feed network, it appears to be very difficult to reduce both amplitude and phase errors simultaneously.
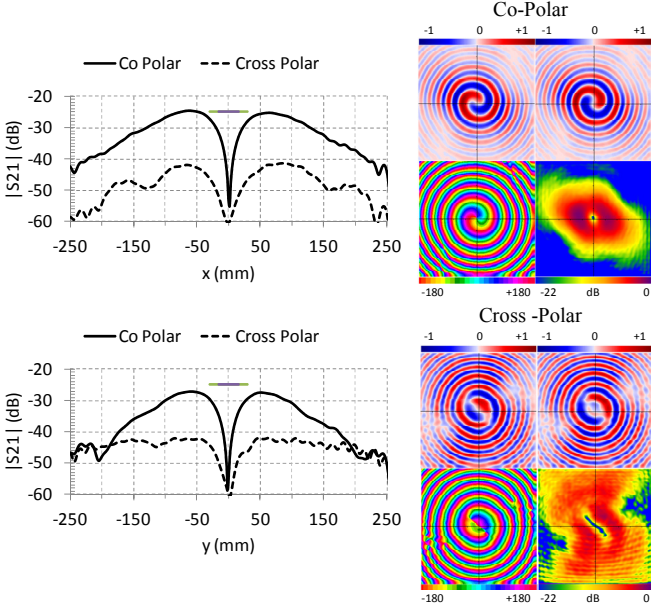

Fig. 7. Beam profile M1 measured at 9.6 GHz with an open-ended WG probe at a scan distance of 300 mm. Colored plots show real, imaginary (top) and phase and magnitude (22.5dB range) (bottom).
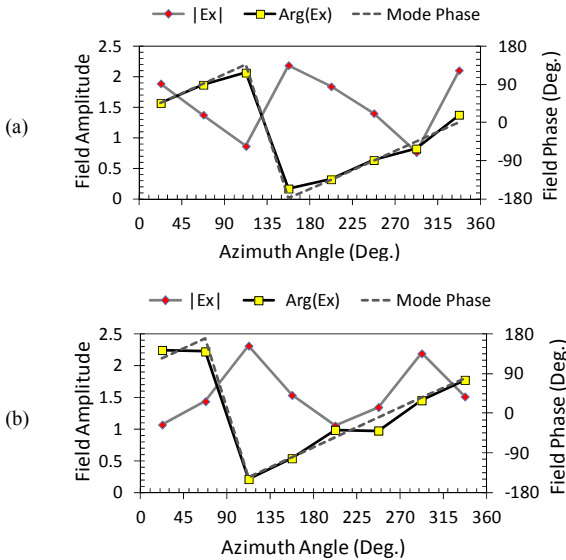

Fig. 8. CFDTD modeled electric field viewed at the eight radiating patch edges opposite their respective feed lines; (a) 10 GHz, (b) 9.6 GHz.

C. Mode Purity of Topological Charge (TC)

The expected TC derived from CFDTD calculations is shown in Fig. 10 where a frequency of approximately 9.5 GHz appears as optimum in the sense of intermodal isolation.

Quantitatively, the mode coupling calculated as $C = TC_{-1}/TC_{+1}$ has a level of -15 dB that agrees well with S-parameter measurements. The TC derived from the measured beam patterns is shown in Fig. 11 and follows the same trend as CFDTD predictions.
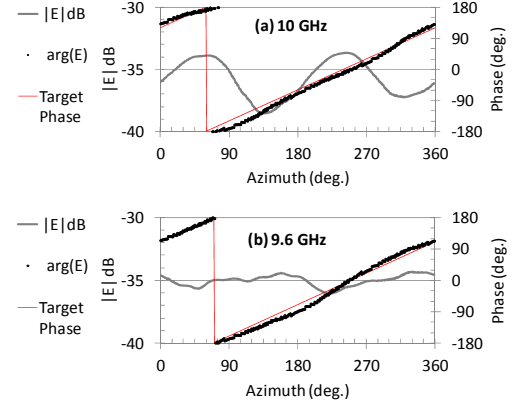

Fig. 9. Measured electric field at a distance of 150 mm using a waveguide probe. Polar radius is 60 mm; (a) 10 GHz, (b) 9.6 GHz.
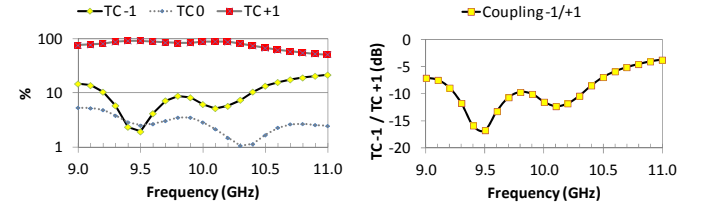

Fig. 10. Topological Charge (TC) calculated from Ex field component simulated by CFDTD for the M1 beam (left) and corresponding Cross Coupling (right). The [ideal] probe is at 60 mm from the M1 aperture.
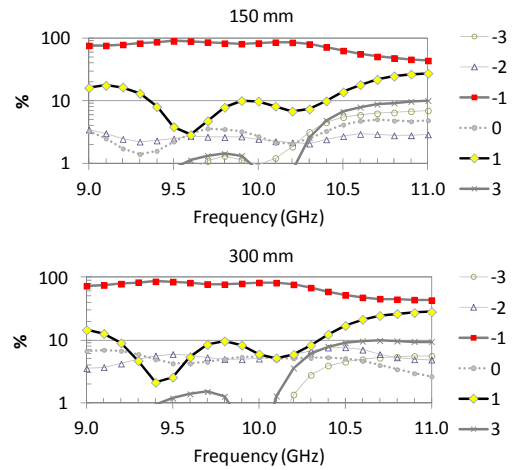

Fig. 11. Topological Charge (TC) calculated from measured copolar field component for the M1 beam at 150 mm (top) and 300 mm (bottom).

D. Mode Convolution Functions (MCF)

The objective here is to demonstrate by comparison with measurements that a simple calculation of the MCF using an ideal aperture, as described in section II.C, is sufficient to obtain the intermodal isolation as well as the power penalty and the reception zone width. Comparisons are shown in Fig. 12 for the 150 mm scan distance and in Fig. 13 for the 300 mm scan distance. In the calculation of MCF an equivalent aperture radius of 25 mm, which is 10% greater than the

maximum extension of the patch slots, was chosen to fit the measured data, with a negative Gaussian amplitude coefficient in equation (6) of $a = -10^3 \text{ m}^{-2}$ to produce a ring of field. Allowing for the fact that the experimental M1 beam is not circularly symmetric, the MCF calculations at both distances conform very well with measurements. This in turn will allow intelligible predictions for the performance of larger arrays at higher frequencies.
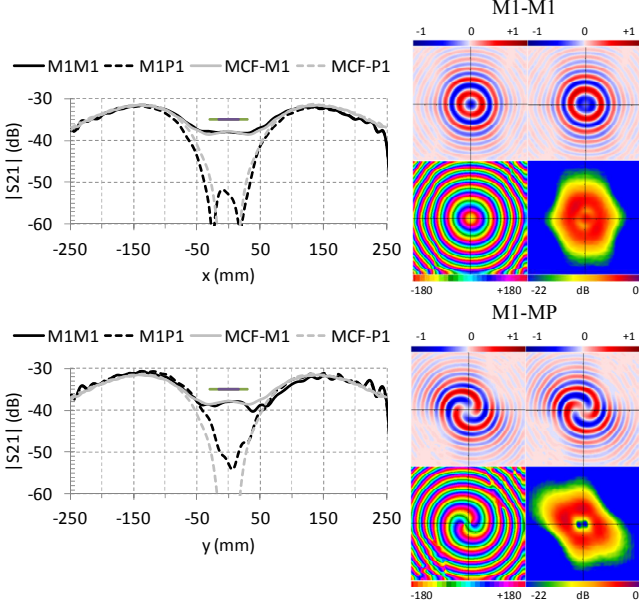

Fig. 12. Reception with a helical mode probe, measured at a scan distance of 150 mm ($\approx 2z_R$). Transmitting mode M1 at 9.6 GHz and receiving either mode M1 or mode P1. MCF refers to the Mode Convolution Function for an ideal beam. Colored plots show real, imaginary (top) and phase and magnitude (22.5dB range) (bottom).

V. DISCUSSION

With the high level of precision obtained in the modeling of input S-parameters, there appears to be a correspondingly high level of agreement between beam measurements and CFDTD calculated field, for both TC and MCF beam classification methods outlined in section II.C. It is more difficult to judge final performance from the beam polar profile presentation, but this is nevertheless very convenient for antenna tuning. As the ASUT used is not ideal, MCF would appear to be a practical test method for classifying helical beam characteristics.

Calculations with the MCF indicate that the power penalty at a range equal to twice the Rayleigh distance is approximately zero dB. At this range the reception width (defined for better than 10 dB isolation) is 0.88 times the effective aperture diameter. Beyond a radius of this width it is impossible to discriminate HB modes. This means that for this technology to work well the HB modes should be concentric such as in the design in [6]. At less than twice the Rayleigh range the power penalty is negative and the antenna system is efficient, behaving as a quasi-optical beam system. At four times the Rayleigh range the power penalty is approximately 6 dB and the reception width (vortex width) is 1.18 times the effective aperture diameter.

The vortex of the UCA antenna is elliptical in shape and this rotates with frequency because of the errors in both patch dimensions and network design. The values of ϵ_r and tanδ obtained from CFDTD have been used in an improved prototype that behaves correctly and will be reported in future work.

In an attempt to extrapolate M1/P1 performance to higher frequencies and larger apertures, consider doubling the aperture diameter to 100 mm, which at 330 GHz would have a Rayleigh range of $z_R = 8.6$ m and at a range of $10z_R = 86$ m the ideal case power penalty would be 16 dB with a reception zone width of 150 mm for greater than 15 dB inter-modal isolation.
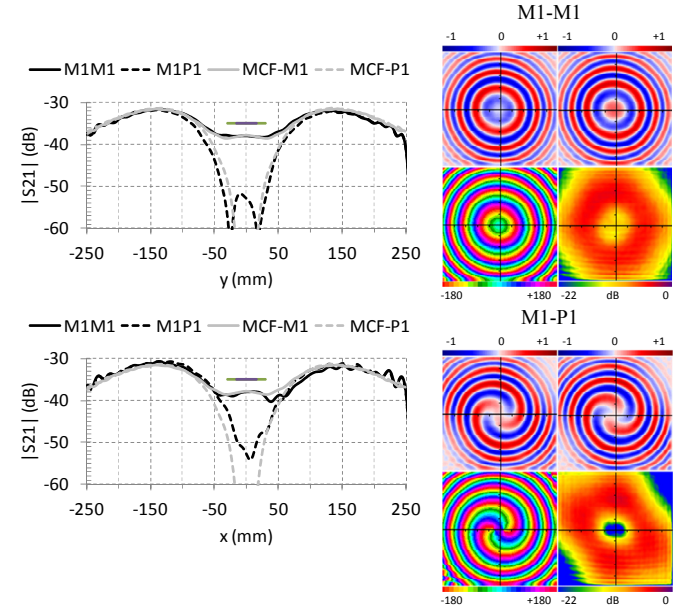

Fig. 13. Reception with helical mode probes, measured at a scan distance of 300 mm. Transmitting mode M1 at 9.6 GHz and receiving mode M1 or mode P1. MCF refers to the Mode Convolution Function for an ideal beam, calculated with a 512×512 point FFT. Colored plots show real, imaginary (top) and phase and magnitude (22.5dB range) (bottom).

VI. CONCLUSIONS

A thorough numerical analysis of the prototype antennas using CFDTD to determine PCB board parameters and FEKO to verify modeling through independent numerical method has in turn enabled the verification of measurements with a planar scanner. Insight into some design flaws and their effect on beam purity have been gained during the process, in particular the limited space for the feed network and its inherent asymmetry lead to the formation of standing waves on the feed lines and corresponding variation in patch excitation, which appears to be difficult to control in practice.

The measurement of helical beam patterns with two opposite mode helical beam probes has inspired a new method for assessing the performance of the radio-link, referred to here as the Mode Convolution Function. This function can be calculated using measured beam patterns with a waveguide probe or for an ideal aperture of equivalent radius. As the calculation is FFT based, a good estimate of intra-modal isolation, power penalty and reception zone area can be

achieved quickly.

MCF calculations suggest that a link distance of ten times the Rayleigh range may be possible if a power penalty of 16 dB can be tolerated, provided HB modes are concentric. However, for optimum link performance with on-axis peak reception the link distance is less than twice the Rayleigh range.

This paper was auto-limited to considering only mode 1 antennas because of the available test antennas but the assessment method could be applied to any mode or polarization.

REFERENCES

[1] L. Allen, M. W. Beijersbergen, R. J. C. Spreeuw, and J. P. Woerdman, " Orbital angular momentum of light and the transformation of Laguerre-Gaussian laser modes", Phys. Rev. A Vol. 45, Iss. 11, pp. 8185-8189, June 1992.

[2] O. Edfors, A.J. Johansson, "Is Orbital Angular Momentum (OAM) Based Radio Communication an Unexploited Area?", IEEE Trans. Antennas Propag, Vol. 60, Nº. 2, pp. 1126-1131, Feb 2012.

[3] B. Thidé, H. Then, J. Sjöholm, K. Palmer, J. Bergman, T.D. Carozzi, Y. N. Istomin, N. H. Ibragimov, and R. Khamitova, "Utilization of photon orbital angular momentum in the low-frequency radio domain," Phys. Rev. Lett., vol. 99, no. 8, pp. 087701-1–087701-4, Aug. 2007.

[4] Q. Bai, A. Tennant, E. Cano, B. Allen, "An experimental phased array for OAM generation", Antennas and Propagation Conference (LAPC), 2014 Loughborough, Nov. 2014.

[5] Z. Zhang, S. Xiao, Yan Li, and Bing-Zhong Wang, "A Circularly Polarized Multimode Patch Antenna for the Generation of Multiple Orbital Angular Momentum Modes", IEEE Antennas Wireless Propag. Lett., Vol. 16, pp. 521-524, 2017.

[6] G. Junkin, "A Circularly Polarized Single Frequency Multimode Helical Beam Antenna", IEEE Transactions on Antennas and Propagation (Early Access), Pages 1-1, DOI: 10.1109/TAP.2018.2883652, 28 November 2018.

[7] M. Albani, A. Mazzinghi, and A. Freni, "Automatic design of CP-RLSA antennas," IEEE Trans. Antennas Propag., vol. 60, no. 12, pp. 5538–5547, Dec. 2012.

[8] D. Comite, G. Valerio, M. Albani, A. Galli, M. Casaletti, and M. Ettorre, "Exciting Vorticity Through Higher Order Bessel Beams With a Radial-Line Slot-Array Antenna", IEEE Trans. Antennas Propag., Vol. 65, Nº. 4, pp. 2123-2128, April 2017.

[9] Clement J. Vourch, Ben Allen, Timothy D. Drysdale, "Planar millimetre-wave antenna simultaneously producing four orbital angular momentum modes and associated multi-element receiver array", IET Microw. Antennas Propag, Vol. 10, Iss. 14, pp. 1492–1499, 2016.

[10] Chen Xu, S. Zheng, W. Zhang, Y. Chen, Hao Chi, X. Jin, and X. Zhang, "Free-Space Radio Communication Employing OAM Multiplexing Based on Rotman Lens", IEEE Microw. Wireless Compon. Lett., Vol. 26, Nº. 9, pp. 738-740, Sept. 2016.

[11] Wenlong Wei, Kourosh Mahdjoubi, Christian Brousseau, Olivier Emile, "Horn antennas for generating radio waves bearing orbital angular momentum by using spiral phase plate", IET Microw. Antennas Propag., Vol. 10, Iss. 13, pp. 1420–1427, 2016.

[12] R. Niemiec, C. Brousseau, K. Mahdjoubi, O. Emile, and A. Ménard "Characterization of an OAM Flat-Plate Antenna in the Millimeter Frequency Band", IEEE Antennas Wireless Propag. Lett., Vol. 13, pp. 1011-1014, 2014.

[13] C. Craeye, "On the Transmittance Between OAM Antennas", IEEE Trans. Antennas Propag., VOL. 64, Nº. 1, Jan. 2016, pp. 336-339.

[14] A. F. Morabito, L Di Donato, and T. Isernia, "Orbital Angular Momentum Antennas: Understanding Actual Possibilities Through the Aperture Antennas Theory ", IEEE Antennas Propag. Mag., Vol. 60, Issue 2, pp. 59–67, Apr. 2018.

[15] Yu Wang, Peng Zhao, et.al. "Integrated photonic emitter with a wide switching range of orbital angular momentum modes", Scientific Reports | 6:22512 | DOI: 10.1038/srep22512, pp. 1–9, 2016.

[16] Goodman, J.W., "Introduction to Fourier Optics", McGraw-Hill, 1st Edition, 1968, (Physical and Quantum Electronics Series). ISBN ISBN-13: 978-0070337766.

[17] D.T. Paris, W.M. Leach, E.B. Joy, "Basic Theory of Probe-Compensated Near-Field Measurements", IEEE Trans. Antennas Propag., Vol. AP-26, Nº.3, May 1978, pp. 373–379.

[18] Junkin, G. "Conformal FDTD Modeling of Imperfect Conductors at Millimeter Wave Bands", IEEE Trans. on Antennas and Propag., Vol. AP-59, Nº 1, Jan. 2011, pp. 199–205.

[19] A.C. Newell, R.D. Ward, E.J. McFarlane, " Gain and Power Parameter Measurements Using Planar Near-Field Techniques", IEEE Trans. Antennas Propag., Vol. AP-36, Nº.6, June 1988, pp. 792–803.

[20] G. Junkin, A. Tennant, "Coefficient compression techniques for conformal FDTD on CUDA devices", Numerical Electromagnetic and Multiphysics Modeling and Optimization for RF, Microwave, and Terahertz Applications (NEMO), 17–19 May 2017.

[21] FEKO https://altairhyperworks.com/product/FEKO.

Gary Junkin (M'98) was born in N. Ireland in 1960. He received the BEng in electronic engineering with communications and PhD in microwave holographic imaging of sub-surface cables, both degrees from the University of Sheffield, Sheffield UK in 1982 and 1986 respectively. He is currently with the Department of Telecommunications and Systems Engineering at the Autonomous University of Barcelona, Catalonia, which he joined in 2002. From 1989 to 1999 he was a lecturer at the Department of Electronic and Electrical Engineering, University of Sheffield, UK. His interests include millimeter-wave holography, phase retrieval, conformal FDTD, mesh generation, and electromagnetic 3D modeling and time-marching field visualization with GPUs.

Josep Parrón was born in Sabadell (Spain) in 1970. He received the Telecommunication Engineer degree and the Doctor Engineer degree from the Universitat Politècnica de Catalunya (UPC), Spain, in 1994 and 2001, respectively. Since 2002, he has been a lecturer in the Department of Telecommunication and Systems Engineering at the Universitat Autònoma de Barcelona (UAB), Spain. His research interests include numerical methods for electromagnetism, antenna design and phased arrays. He is the author or coauthor of more than 80 technical journal articles and conference papers.